Supporting Information

for

The Entatic State of Alternative cofactors. Leveling of Catalytic Properties Among the Metal Ions Variants of Mandelate Racemase

Matthew L. Harty[†], Amar Nath Sharma[†], and Stephen L. Bearne[†,‡,*]

† Department of Biochemistry and Molecular Biology, Dalhousie University, Halifax, NS, B3H 4R2, Canada

‡ Department of Chemistry, Dalhousie University, Halifax, NS, B3H 4R2, Canada

* Author to whom correspondence should be addressed.

Phone: (902) 494-1974; fax: (902) 494-1355; e-mail: sbearne@dal.ca

TABLE OF CONTENTS **PAGE**

Table S1. Activation constants for various cations examined for their ability to activate apo-MR

cation	corresponding salt	K_A (mM)	K_A' (mM)
Li^{+}	$LiCl_2$	–[b]	–
Mg^{2+}	$MgCl_2$	0.394 (± 0.001)	NA[c]
Al^{3+}	$AlCl_3$	–	–
Ca^{2+}	$CaCl_2 \cdot 2H_2O$	–	–
Sc^{3+}	$ScCl_3$	–	–
V^{2+}	VCl_2	–	–
Cr^{2+}	$CrCl_2$	–	–
Cr^{3+}	$CrCl_3 \cdot 6H_2O$	–	–
Mn^{2+}	$MnCl_2 \cdot 4H_2O$	0.040 (± 0.002)	NA
Fe^{2+}	$FeCl_2$	immeasurable[d]	unknown
Co^{2+}	$CoCl_2 \cdot 6H_2O$	0.057 (± 0.004)[e] 0.74 (± 0.17)[f]	4.1 (± 0.6)[e] 0.31 (± 0.05)[f]
Ni^{2+}	$NiCl_2$	0.091 (± 0.001)[e] 1.2 (± 0.1)[f]	11 (± 1)[e] 0.68 (± 0.39)[f]
Cu^{2+}	$CuCl_2$	–	–
Zn^{2+}	$ZnCl_2$	–	–
Sr^{2+}	$SrCl_2$	–	–
Cd^{2+}	$CdCl_2 \cdot 2½H_2O$	–	–
Ba^{2+}	$BaCl_2 \cdot 2H_2O$	–	–
Hg^{2+}	$HgCl_2$	–	–

[a] Values are means of triplicate trials and reported errors are standard deviations.
[b] No activation observed.
[c] Not applicable.
[d] Protein precipitation was observed, giving rise to highly variable ellipicity values in the CD-based assay. The precipitation may arise from the autooxidation of Fe^{2+} to form Fe^{3+} at pH values above 7, and concomitant production of free radicals of HEPES.[1-3]
[e] Eqn. 3 used to fit initial velocity data (second metal binding event).
[f] Eqn. S1 used to fit initial velocity data (substrate depletion).

Table S2. Selected properties of Mg^{2+}, Mn^{2+}, Co^{2+}, and Ni^{2+}

Property	Mg^{2+}	Mn^{2+}	Co^{2+}	Ni^{2+}
ionic radius, R (Å)[a]	0.72	0.83 (H.S.)[o] 0.67 (L.S.)	0.75 (H.S.) 0.65 (L.S.)	0.69
M^{2+}–O distance in aqueous solution (Å)[b]	2.10	2.20	2.08	2.055
$\Delta G_{hydration}$ (kcal/mol)[c]	–19.75	–18.98	–20.79	–21.43
cytosolic concentration (M)	10^{-3}[d]	10^{-6}[e]	10^{-9}[f]	10^{-9}[g]
electron affinity (eV)[h] (kcal/mol)	15.04 (346.8)	15.64 (360.7)	17.06 (393.4)	18.17 (419.0)
ionization potential (eV)[h]	80.14	33.67	33.5	35.17
electronegativity (eV)[h] (kcal/mol)	47.59 (1097.45)	24.66 (568.67)	25.28 (582.97)	26.67 (615.03)
absolute hardness (eV)[h]	32.55	9.02	8.22	8.5
calculated Z_{eff} for the valence shell[i]	2.85	5.60	6.90	7.55
ionic potential, Z_{eff}^2/R ($Å^{-1}$)	11.3	37.8	63.5	82.6
Coulombic potential, $\Gamma = Z_{eff}/R^2$ ($Å^{-2}$)[j]	5.50	8.13	12.27	15.85
Stability constants for binding BzH in assay buffer (M^{-1})[k]	$K_1 = 83 \pm 6$	$K_1 = 206 \pm 35$ $K_2 = 68 \pm 13$	$K_1 = 2.1 (\pm 0.6) \times 10^3$ $K_2 = 5.9 (\pm 0.5) \times 10^3$	$K_1 = 1.5 (\pm 0.4) \times 10^4$ $K_2 = 842 \pm 101$
Stability constants for binding BzP in assay buffer (M^{-1})[k]	–	–	–	$K_1 = 515 \pm 10$
Stability constants for binding F^- in aqueous solution (M^{-1})[l] (all values I = 1.0 M at 25 °C) (kcal/mol)	20.9 ± 1.1 (–1.80 ± 0.03)	6.17 ± 0.71 (–1.08 ± 0.07)	2.7 ± 0.4 (–0.59 ± 0.09)	4.6 ± 0.5 (–0.90 ± 0.06)
Stability constants for binding ETDA (M^{-1})[m] (all values I = 0.1 M at 25 °C) (kcal/mol)	8.79 (–11.99)	13.89 (–18.55)	16.45 (–22.44)	18.4 (–25.10)
Stability constants for binding NTA (M^{-1})[n] (all values I = 0.1 M at 20 °C) (kcal/mol)	5.46 (–7.45)	7.44 (–10.15)	10.38 (–14.16)	11.54 (–15.74)
metal complex constants (MC)[o]	–0.12	0.55	0.91	1.20

[a] From ref. 4; [b] From refs. 5 and 6; [c] From ref. 7; [d] From ref. 8; [e] From ref. 9; [f] From ref. 10; [g] From ref. 11; [h] From ref. 12; [i] Effective nuclear charge (Z_{eff}) calculated using Slater's rules.[13]; [j] Calculated from data in this table based on ref. 14; [k] From ref. 15; [l] From refs. 16 [MgF^+, I = 1.0 M, 25 °C; other values (M^{-1}) include 22.9 ± 0.1 at 25 °C and I = 0.7 from ref. 17 and 28.7 ± 1.7, 22.0 ± 1.6, 18.8 ± 0.7, and 18.6 ± 0.8 at 25 °C and I = 0.1, 0.4, 0.7, and 1.0 M, respectively, from ref. 18], 19 (MnF^+, I =1.0 M, 25 °C), 20 (CoF^+, I =1.0 M, 25 °C), and 21 (NiF^+, I =1.0 M, 25 °C); [m] From ref. 22; [n] From ref. 23 and ΔG values calculated at 25 °C; [o] From ref. 24; [p] H.S. and L.S. denote high spin and low spin, respectively.

Table S3. Free energy changes for the racemization of (*R*)- and (*S*)-mandelate catalyzed by the metal ion variants of MR

Metal ion	Mg^{2+}	Mn^{2+}	Co^{2+}	Ni^{2+}
ΔG_R (kcal/mol)[b]	–4.12 ± 0.04[a]	–3.96 ± 0.05	–4.04 ± 0.03	–4.09 ± 0.03
$\Delta G^{\ddagger}_{ER}$ (kcal/mol)	13.53 ± 0.01	14.70 ± 0.03	13.70 ± 0.03	13.76 ± 0.02
$\Delta G^{\ddagger}_{E+R}$ (kcal/mol)	9.42 ± 0.04	10.74 ± 0.06	9.68 ± 0.05	9.69 ± 0.04
ΔG_S (kcal/mol)	–4.30 ± 0.06	–4.65 ± 0.03	–4.43 ± 0.06	–4.34 ± 0.03
$\Delta G^{\ddagger}_{ES}$ (kcal/mol)	13.72 ± 0.02	14.93 ± 0.01	13.84 ± 0.02	13.82 ± 0.04
$\Delta G^{\ddagger}_{E+S}$ (kcal/mol)	9.44 ± 0.06	10.29 ± 0.03	9.43 ± 0.07	9.49 ± 0.04
ΔG_A (kcal/mol)	–4.64 ± 0.01	–6.0 ± 0.03	–5.79 ± 0.04	–5.51 ± 0.01
ΔG_{eq} (kcal/mol)	0.02 ± 0.08	–0.45 ± 0.06	–0.24 ± 0.08	–0.20 ± 0.05

[a] Values are calculated from kinetic parameters presented in **Table 1** using $\Delta G = RT\ln K$, where K is a dissociation constant, and $\Delta G^{\ddagger} = RT\ln(k_B T/h) - RT\ln k$, where k_B is the Boltzmann constant, h is Planck's constant, and k is the apparent rate constant k_{cat} or k_{cat}/K_m.

[b] Meanings of the subscripts: R and S refer to (*R*)- and (*S*)-mandelate, respectively; E is the enzyme; ER and ES are the respective enzyme-substrate complexes; A refers to activation by the metal ion calculated based on $1/K_1$ (**Supplementary Table S2**), and eq refers to the overall equilibrium (i.e., K_{eq} = [S]/[R]).

Table S4. Free energy changes accompanying racemization of (*S*)-TFLA catalyzed by the metal ion variants of MR[a]

Metal ion	ΔG_T (kcal/mol)	$\Delta G^{\ddagger}_{ET}$ (kcal/mol)	$\Delta G^{\ddagger}_{E+T}$ (kcal/mol)
Mg^{2+}	–3.84 ± 0.01	17.09 ± 0.04	13.28 ± 0.04
Mn^{2+}	–3.53 ± 0.09	17.13 ± 0.03	13.7 ± 0.1
Co^{2+}	–3.85 ± 0.08	16.83 ± 0.08	12.9 ± 0.1
Ni^{2+}	–3.74 ± 0.03	16.83 ± 0.02	13.12 ± 0.04

[a] Values are means of triplicate trials and reported errors are standard deviations and are calculated from the kinetic parameters in **Table 2**. The subscripts T and E refer to (*S*)-TFLA and metal ion enzyme variant, respectively.

Table S5. Free energy changes accompanying binding of BzH with MR and with metal ion (M^{2+})

Metal ion[a]	**Mg^{2+}**	**Mn^{2+}**	**Co^{2+}**	**Ni^{2+}**
ΔG_A (kcal/mol)[b]	–4.64 ± 0.01	–6.00 ± 0.03	–5.79 ± 0.04	–5.51 ± 0.01
ΔG_d (kcal/mol)[c]	–2.62 ± 0.04	–3.2 ± 0.1	–4.5 ± 0.2	–5.7 ± 0.2
ΔG_i (kcal/mol)[d]	–6.75 ± 0.01	–6.67 ± 0.09	–7.02 ± 0.03	–7.60 ± 0.02
$\Delta\Delta G_{M^{2+}}$ (kcal/mol)[e]	4.13 ± 0.04	3.5 ± 0.1	2.5 ± 0.2	1.9 ± 0.2

[a] Meanings of the subscripts: A refers to activation by the metal ion calculated based on $1/K_1$ (**Supplementary Table S2**), d refers the free energy change accompanying formation of the M^{2+}·BzH complex, and I refers to the free energy change accompanying formation of the M^{2+}-MR·BzH.

[b] Values are calculated from K_A values presented in **Table 1**.

[c] Values calculated from the association constants (K_1) of M^{2+} with BzH from ref. 15. See **Supplementary Table S2**.

[d] Values calculated from K_i values presented in **Table 3**.

[e] $\Delta\Delta G_{M2+} = \Delta G_d - \Delta G_i$.

Table S6. Examples of enzymes activated by binding Mg^{2+}, Mn^{2+}, Co^{2+}, and Ni^{2+}, which exhibit ≤ 10-fold change in kinetic constants for the various metal ion variants[(a)]

Enzyme	activity (based on V_{max} or k_{cat} data)	K_m	reference
hydrogen hydrogenase (EC 1.12.1.2)[b]	Ni^{2+} (100) ≈ Co^{2+} (98) ≈ Mg^{2+} (86) > Mn^{2+} (36) **(2.8-fold)**	–	25
3-methyl-2-oxobutanoate hydroxymethyltransferase (EC 2.1.2.11)[b]	Mg^{2+} (100) > Mn^{2+} (75) > Ni^{2+} (57) ≈ Co^{2+} (51) **(2.1-fold)**	–	26
glycoprotein 3-α-L-fucosyltransferase (AgFucTA) (EC 2.4.1.214)[b]	Mn^{2+} (100) > Mg^{2+} (49) ≈ Ni^{2+} (42) > Co^{2+} (28) **(3.6-fold)**	–	27
monogalactosyldiacylglycerol synthase (EC 2.4.1.46)[b]	Mn^{2+} (100) > Co^{2+} (71) ≈ Mn^{2+} (67) > Ni^{2+} (44) **(2.3-fold)**		28
glucosyl-3-phosphoglycerate synthase (GpgS) (EC 2.4.1.266)[b]	Mg^{2+} (100) > Mn^{2+} (75) ≈ Co^{2+} (60) > Ni^{2+} (27) **(3.7-fold)**	–	29
mannosylglucosyl-3-phosphoglycerate synthease (MggB) (EC 2.4.1.270)[b]	Mg^{2+} (100) > Ni^{2+} (73) ≈ Co^{2+} (67) > Mn^{2+} (45) **(2.2-fold)**	–	29
pseudaminic acid synthase (EC 2.5.1.97)[b]	Co^{2+} (100) ≈ Mn^{2+} (91) > Mg^{2+} (48) > Ni^{2+} (26) **(3.8-fold)**	–	30
protein tyrosine kinase CSK (EC 2.7.10.2)[c]	Mg^{2+} (100) > Co^{2+} (69) > Mn^{2+} (14) > Ni^{2+} (40) **(7.1-fold)**	Mg^{2+} (100) > Ni^{2+} (33) > Co^{2+} (22) > Mn^{2+} (7) (poly(E,Y))	31
protein-serine/threonine phosphatase (EC 3.1.3.16)[b]	Mn^{2+} (100) ≈ Ni^{2+} (84) > Mg^{2+} (61) > Co^{2+} (33) **(3.0-fold)**	–	32
pyridoxal phosphatase (EC 3.1.3.74)[c]	Ni^{2+} (100) ≈ Co^{2+} (87) ≈ Mg^{2+} (78) > Mn^{2+} (18) **(5.5-fold)**	Co^{2+} (100) ≈ Mg^{2+} (93)	33
dihydroxy acid dehydratase (EC 4.2.1.9)[b]	Co^{2+} (100) ≈ Ni^{2+} (82) ≈ Mn^{2+} (71) ≈ Mg^{2+} (71) **(1.4-fold)**	–	34
4-hydroxy-4-methyl-2-oxoglutarate (HMG)/4-carboxy-4-hydroxy-2-oxoadipate aldolases (OAA) (EC 4.1.3.17/B3)[b]	Mg^{2+} (100) ≈ Mn^{2+} (90) > Co^{2+} (65) > Ni^{2+} (28) **(HMG, 3.6-fold)** Ni^{2+} (100) > Co^{2+} (75) > Mg^{2+} (40) > Mn^{2+} (23) **(OAA, 4.3-fold)**	–	35
4-hydroxy-2-oxovalerate aldolase (EC 4.1.3.39)[b]	Mn^{2+} (100) > Ni^{2+} (76) > Co^{2+} (60) > Mg^{2+} (35) **(2.9-fold)**	–	36
D-threonine aldolase (EC 4.1.2.42)[b]	Mn^{2+} (100) ≈ Co^{2+} (94) ≈ Mg^{2+} (92) ≈ Ni^{2+} (85) **(1.2-fold)**	–	37
(*R*)-citramalyl-CoA lyase (EC 4.1.3.46)[b]	Mn^{2+} (100) ≈ Co^{2+} (100) > Ni^{2+} (75) > Mg^{2+} (60) **(1.7-fold)**	–	38

N-acylphosphatidylethanolamine-hydrolyzing phospholipase D (EC 4.1.4.4)[b]	Mg^{2+} (100) > Co^{2+} (75) ≈ Ni^{2+} (71) > Mn^{2+} (36) **(2.8-fold)**	–	39
rat erythrocyte glyoxylase I (EC 4.4.1.5)[c]	Mg^{2+} (100) ≈ Co^{2+} (85) > Mn^{2+} (46) ≈ Ni^{2+} (40) **(2.5-fold)**	Mg^{2+} (100) > Mn^{2+} (56) ≈ Co^{2+} (44) = Ni^{2+} (44)	40
isopentenyl diphosphate Δ-isomerase (EC 5.3.3.2)[b]	Ni^{2+} (100) ≈ Co^{2+} (88) > Mg^{2+} (65) > Mn^{2+} (47) **(2.1-fold)**	–	41
α-phosphoglucomutase (EC 5.4.2.2)[b]	Co^{2+} (100) > Mn^{2+} (70) > Mg^{2+} (25) ≈ Ni^{2+} (23) **(4.3-fold)**	–	42
β-phosphoglucomutase (EC 5.4.2.6)[b]	Co^{2+} (100) > Mn^{2+} (68) ≈ Mg^{2+} (68) > Ni^{2+} (40) **(2.5-fold)**	–	43
phosphoenolpyruvate mutase (EC 5.4.2.9)[b]	Mg^{2+} (100) ≈ Co^{2+} (70) ≈ Ni^{2+} (60) > Mn^{2+} (30) **(3.3-fold)**	–	44
D-psicose 3-epimerase (EC 5.5.1.30)[b]	Co^{2+} (100) ≈ Mn^{2+} (92) > Ni^{2+} (65) > Mg^{2+} (38) **(2.6-fold)**	–	45,46
AMP-forming acetyl-CoA synthase (EC 6.2.1.1)[b]	Mg^{2+} (100) ≈ Mn^{2+} (94) ≈ Co^{2+} (82) > Ni^{2+} (27) **(3.7-fold)**	–	47
biotin-[methylmalonyl-CoA-carboxytransferase] (EC 6.3.4.9)[b]	Mn^{2+} (100) > Co^{2+} (90) ≈ Mg^{2+} (90) > Ni^{2+} (70) **(1.4-fold)**	–	48

[a] Where possible, enzymes that recognize substrates only when the substrates are complexed with the divalent metal ions are not included, although this is not always clear in many reports. Data for other divalent metal ions that may serve as activators are not presented.

[b] Based on specific activity measurements or reported relative activities.

[c] Based on measured V_{max} or k_{cat} values and K_m values.

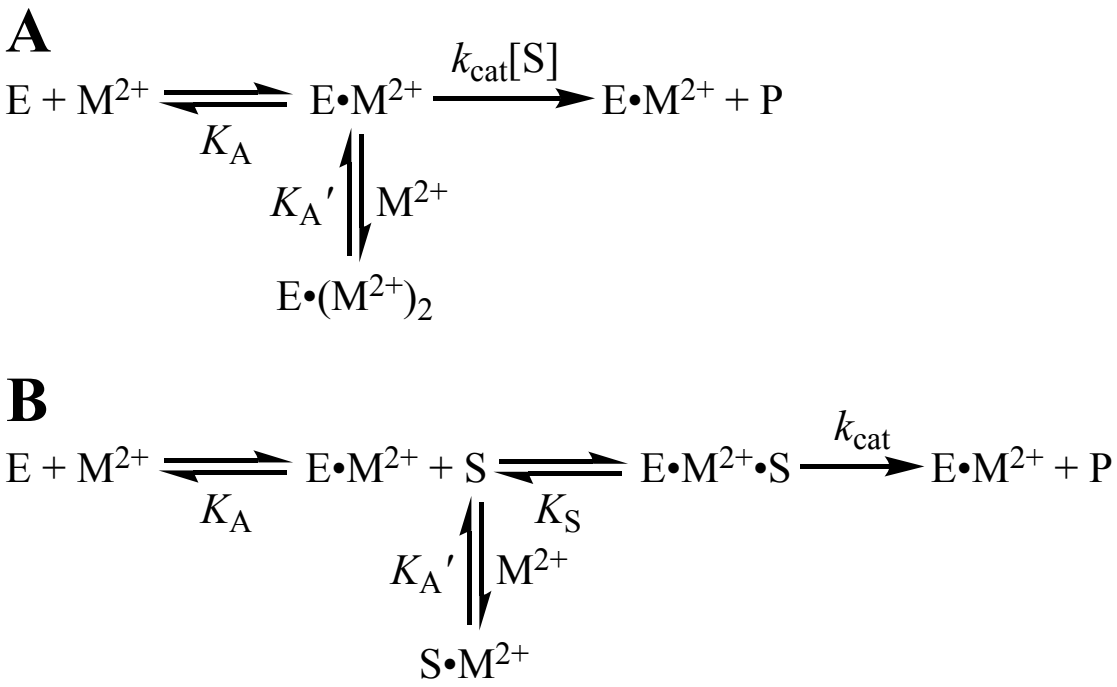

Supplementary Scheme S1. Two kinetic mechanisms that could account for the observed inhibition of MR activity at elevated concentrations of Co^{2+} and Ni^{2+} include (**A**) the binding of a second metal ion giving rise to an inactive ternary complex under saturating concentrations of substrate, or (**B**) interaction of the metal ions with the substrate to yield a complex between mandelate and the metal ion that is not recognized as a substrate.

Inhibition mechanism 1. At saturating concentrations of substrate, the initial velocity equations corresponding to **Supplementary Scheme S1A** are given by eqns. 2 (no second binding event) and 3 (binding of a second metal ion).

$$v_{\mathrm{i}} = \frac{V_{\max}[\mathrm{M}^{2+}]}{K_{\mathrm{A}}+[\mathrm{M}^{2+}]} \tag{2}$$

$$v_{\mathrm{i}} = \frac{V_{\max}[\mathrm{M}^{2+}]}{K_{\mathrm{A}}+[\mathrm{M}^{2+}]\left(1+\frac{[\mathrm{M}^{2+}]}{K'_{\mathrm{A}}}\right)} \tag{3}$$

Inhibition mechanism 2. The initial velocity equation corresponding to **Supplementary Scheme S1B** is given by eqn. S1,

$$v_{\mathrm{i}} = \frac{V_{\max}\left(\frac{[\mathrm{S}]}{K_{\mathrm{S}}+[\mathrm{S}]}\right)[\mathrm{M}^{2+}]}{K_{\mathrm{A}}\left(\frac{K_{\mathrm{S}}}{K_{\mathrm{S}}+[\mathrm{S}]}\right)+[\mathrm{M}^{2+}]} \tag{S1}$$

where the concentration of free substrate ([S]) is related to the total concentration of substrate ($[\mathrm{S}]_{\mathrm{T}} = [\mathrm{S}] + [\mathrm{S}\cdot\mathrm{M}^{2+}]$) by eqn. S2.

$$[\mathrm{S}] = [\mathrm{S}]_{\mathrm{T}}\left(\frac{K'_{\mathrm{A}}}{K'_{\mathrm{A}}+[\mathrm{M}^{2+}]}\right) \tag{S2}$$

For fitting of eqn. S1 to the initial velocity data for the activation of apo-MR by Co^{2+} and Ni^{2+}, using nonlinear regression analysis, the values of $[\mathrm{S}]_{\mathrm{T}}$ and K_{S} were fixed at 10.0 mM and 1.0 mM, respectively (**Supplementary Fig. S2**).

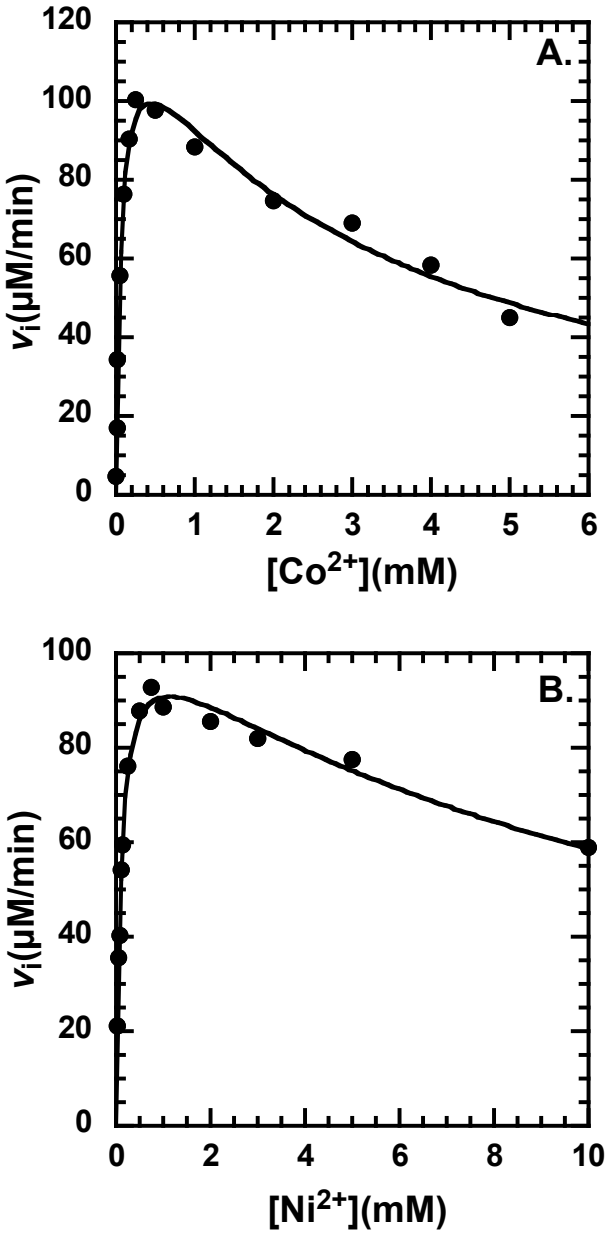

Supplementary Figure S1. Representative plots for the activation of apo-MR by Co^{2+} (**A**) and Ni^{2+} (**B**). MR (0.2 μg/mL, i.e., 4.85 μM) was incubated for 20 min with varying concentrations of the respective metal ion prior to addition of a saturating concentration of substrate (*R*)-mandelate (10 mM). Activation constants (K_A and K_A') were determined using eqn. 3 and are presented in **Supplementary Table S1**.

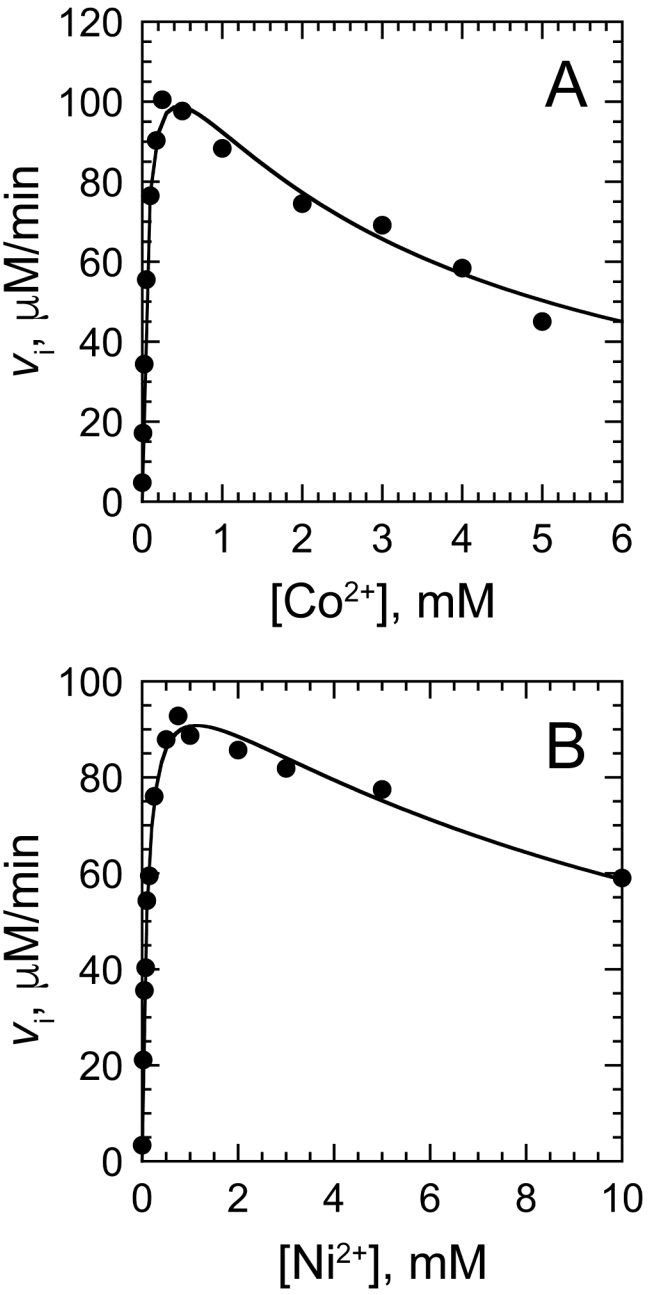

Supplementary Figure S2. Representative plots for the activation of apo-MR by Co^{2+} (**A**) and Ni^{2+} (**B**) using the same data as in **Supplementary Figure S1**. Eqn. S1 was used to fit the initial velocity data and to determine K_A and K_A'. Values are listed in **Supplementary Table S1**.

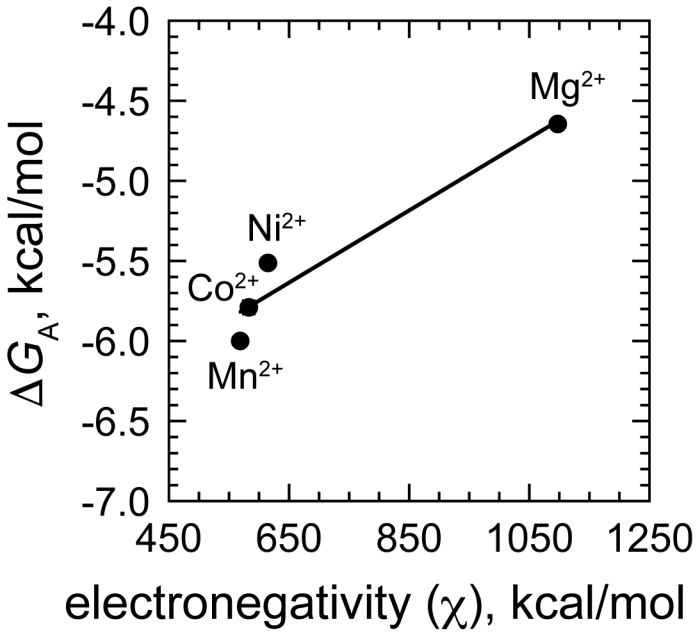

Supplementary Figure S3. Weak correlation ($R^2 = 0.9308$) between the free energy of activation (ΔG_A) by the metal ions and the electronegativity (χ).

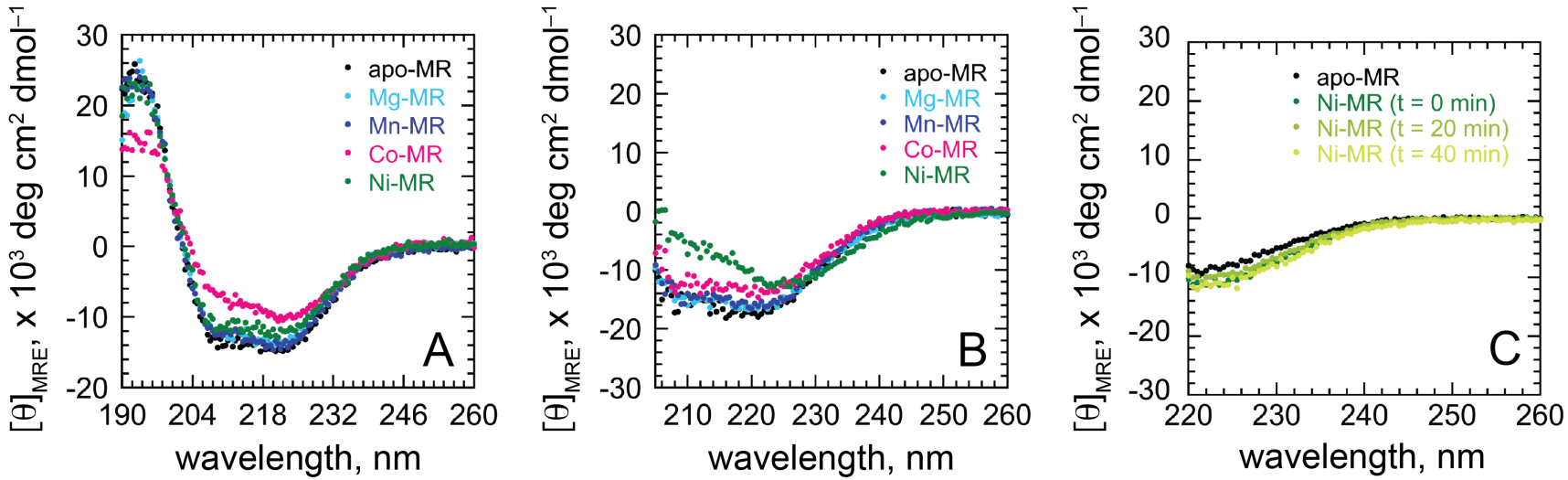

Supplementary Figure S4. CD spectra for apo-MR, and Mg^{2+}-bound, Mn^{2+}-bound, Co^{2+}-bound, and Ni^{2+}-bound MR. The mean residue ellipticities ($[\theta]_{MRE} = \theta/(l \cdot c \cdot n)$ where l = 0.1 cm, c = 65 μg/mL (1.58 μM), and n = 383 amino acid residues) are plotted as a function of wavelength for metal ion-free (apo) MR (black), and MR in presence of Mg^{2+} (3.9 mM, cyan), Mn^{2+} (0.4 mM, blue), Co^{2+} (0.5 mM, pink), and Ni^{2+} (0.9 mM, green) at 25 °C. Panel **A** shows the CD spectra recorded in Na^{+}-phosphate buffer (25 mM, pH 7.5). While there were no significant differences of the CD spectra for apo-MR, Mg^{2+}-MR, Mn^{2+}-MR, and Ni^{2+}-MR, the spectrum for Co^{2+}-MR exhibited a time dependence that resulted in an upward shift of the spectra at λ between 204 and 226 nm. The spectrum shown for Co^{2+}-MR is the one obtained immediately after mixing apo-MR with the Co^{2+}-containing stock solution. Panel **B** shows the CD spectra recorded in Na^{+}-HEPES buffer (10 mM, pH 7.5). In this buffer, no significant differences of the CD spectra for apo-MR, Mg^{2+}-MR, Mn^{2+}-MR, and Co^{2+}-MR were observed. However, the CD spectrum of Ni^{2+}-MR exhibited a time dependence that resulted in an upward

shift of the spectra at λ between 204 and 226 nm, while the CD spectrum of Co^{2+}-MR did not. The spectrum shown for Ni^{2+}-MR is the one obtained immediately after mixing apo-MR with the Ni^{2+}-containing stock solution. Panel **C** shows the CD spectra recorded in Na^{+}-HEPES buffer (100 mM, pH 7.5). This buffer concentration was examined because it is identical to the buffer system used in the enzymatic assays despite having the spectra truncated at 220 nm due to a lack of buffer transparency. In this buffer, the CD spectrum of Ni^{2+}-MR was similar to that of apo-MR and no time dependent changes in the spectrum were observed over 40 min.

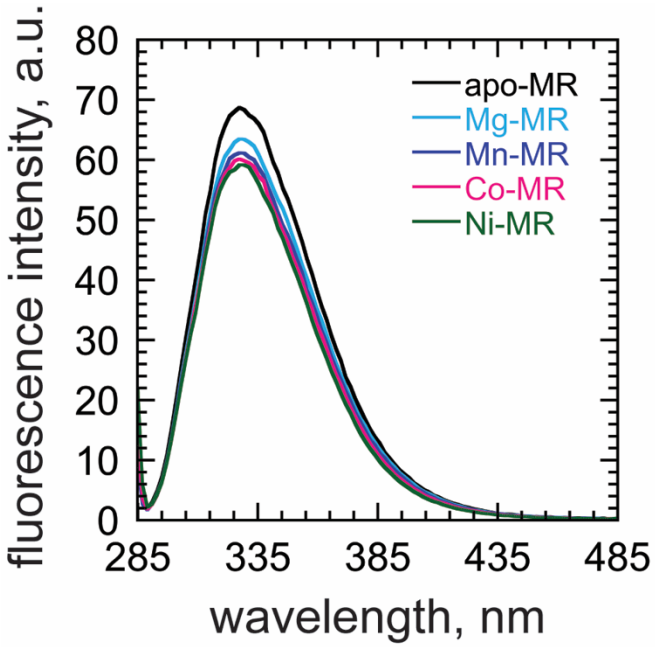

Supplementary Figure S5. Fluorescence spectra for apo-MR, and Mg^{2+}-bound, Mn^{2+}-bound, Co^{2+}-bound, and Ni^{2+}-bound MR. Intrinsic fluorescence spectra (285 – 485 nm) were obtained using λ_{ex} = 280 nm. The spectra for metal ion-free (apo) MR (black), and MR in presence of Mg^{2+} (3.9 mM, cyan), Mn^{2+} (0.4 mM, blue), Co^{2+} (0.5 mM, pink), and Ni^{2+} (0.9 mM, green) in Na^{+}-HEPES buffer (100 mM, pH 7.5) are shown. The protein concentration is 1.0 μM. At protein concentrations >5.0 μM, slight precipitation of the Ni^{2+}-MR was observed; however, assay concentrations of Ni^{2+}-MR (i.e., ~5 nM) were ~1000-fold lower than the concentrations where protein precipitation occurs (i.e., ~5 μM).

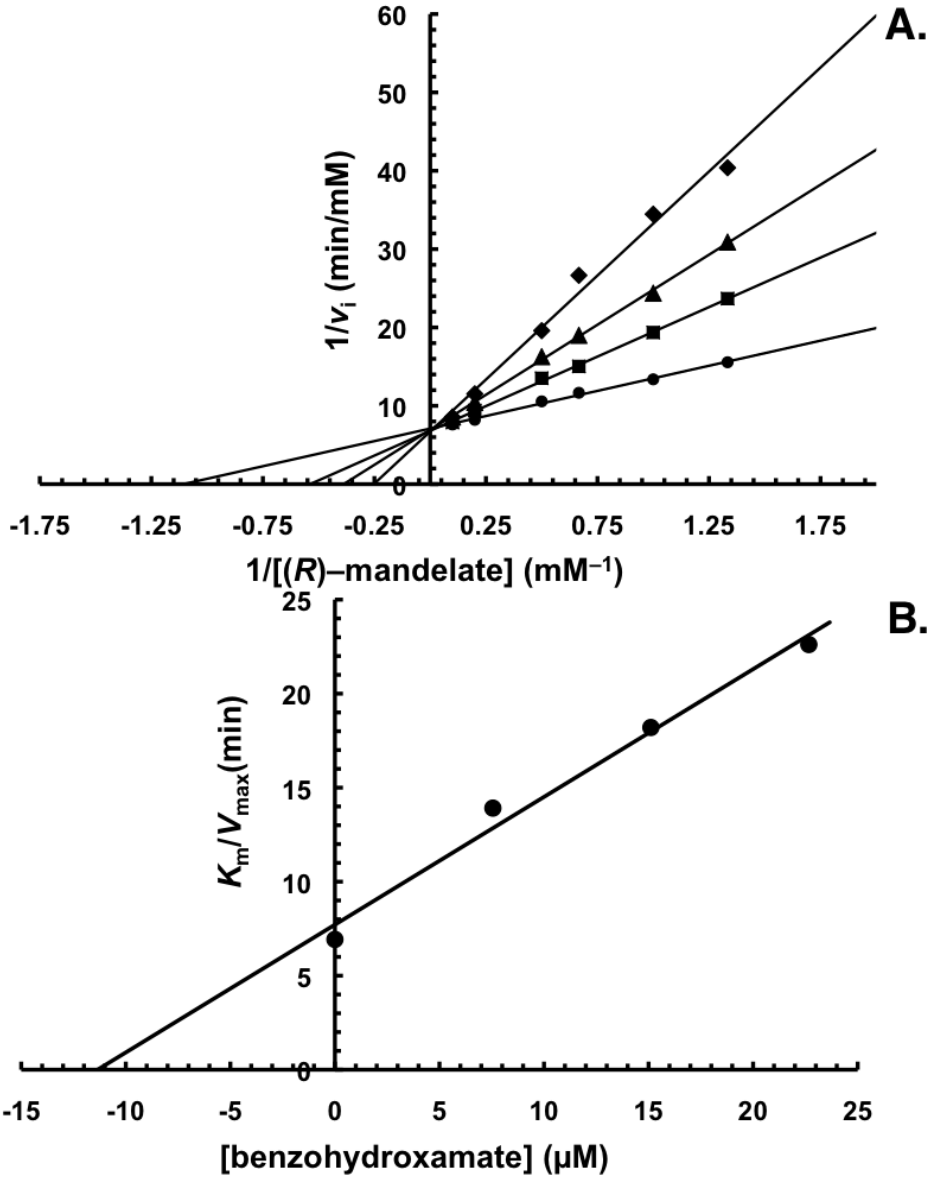

Supplementary Figure S6. A representative double reciprocal plot for the competitive inhibition of Mg^{2+}-bound MR by BzH (**A**) and replot of $(K_m/V_{max})^{app}$ as a function of free BzH concentrations (**B**). (**A**) Initial concentrations of (*R*)-mandelate ranged between values of 0.75 mM and 10.00 mM. Concentrations of total BzH used were 0 μM (●), 10 μM (■), 20 μM (▲), and 30 μM (◆). Assay conditions were as described in the Materials & Methods. (**B**) Re-plot of $(K_m/V_{max})^{app}$ values (determined from nonlinear regression analysis) as a function of free BzH concentrations ($[I]_{free}$ = 7.5, 15.1, and 22.6 μM) as determined by the method described in the Materials & Methods. The K_i value determined from these plots is 11.3 ± 0.2 μM.

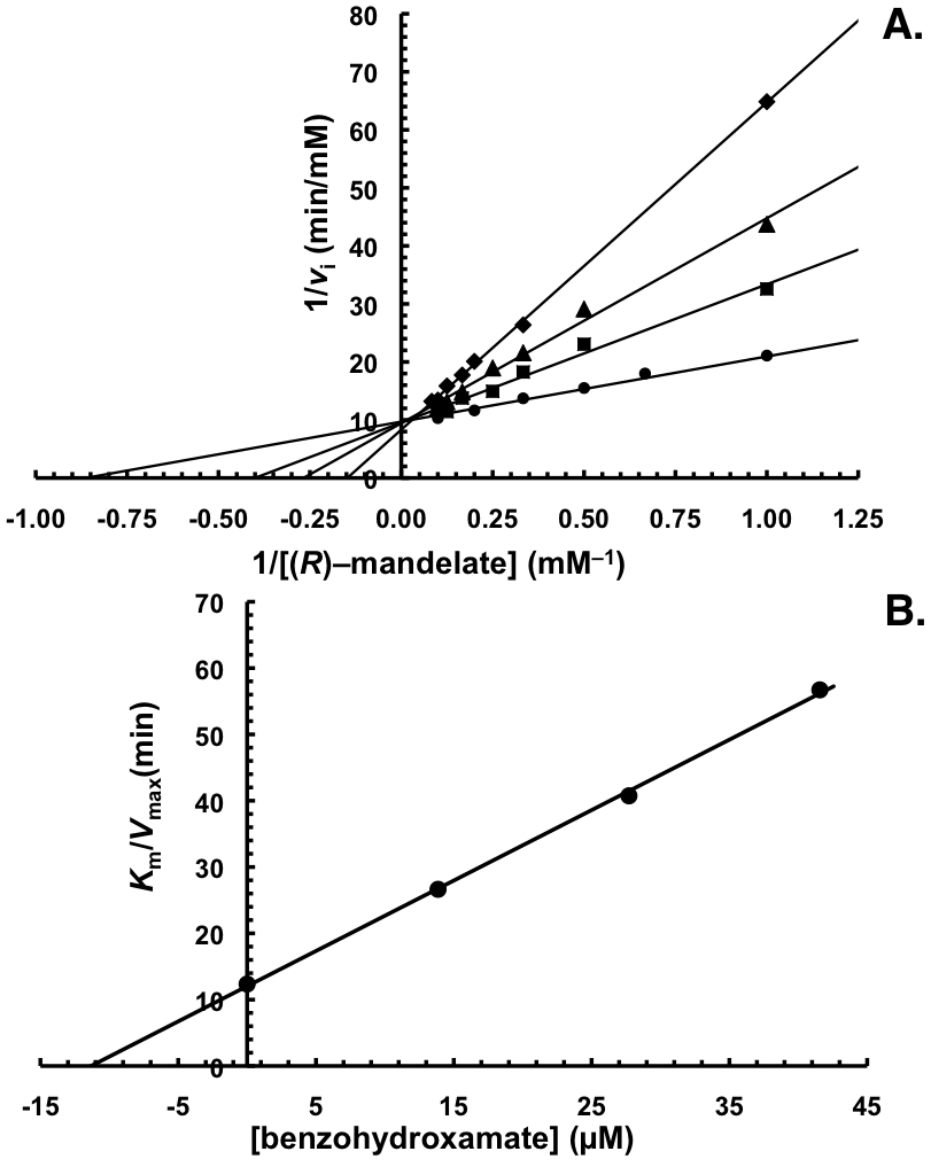

Supplementary Figure S7. A representative double reciprocal plot for the competitive inhibition of Mn^{2+}-bound MR by BzH (**A**) and replot of $(K_m/V_{max})^{app}$ as a function of free BzH concentrations (**B**). (**A**) Initial concentrations of (*R*)-mandelate ranged between values of 1.00 mM and 10.00 mM. Concentrations of total BzH used were 0 μM (●), 15 μM (■), 30 μM (▲), and 45 μM (◆). Assay conditions were as described in the Materials & Methods. (**B**) Re-plot of $(K_m/V_{max})^{app}$ values (determined from nonlinear regression analysis) as a function of free BzH concentrations ($[I]_{free}$ = 13.8, 27.7, and 41.5 μM) as determined by the method described in the Materials & Methods. The K_i value determined from these plots is 13 ± 2 μM.

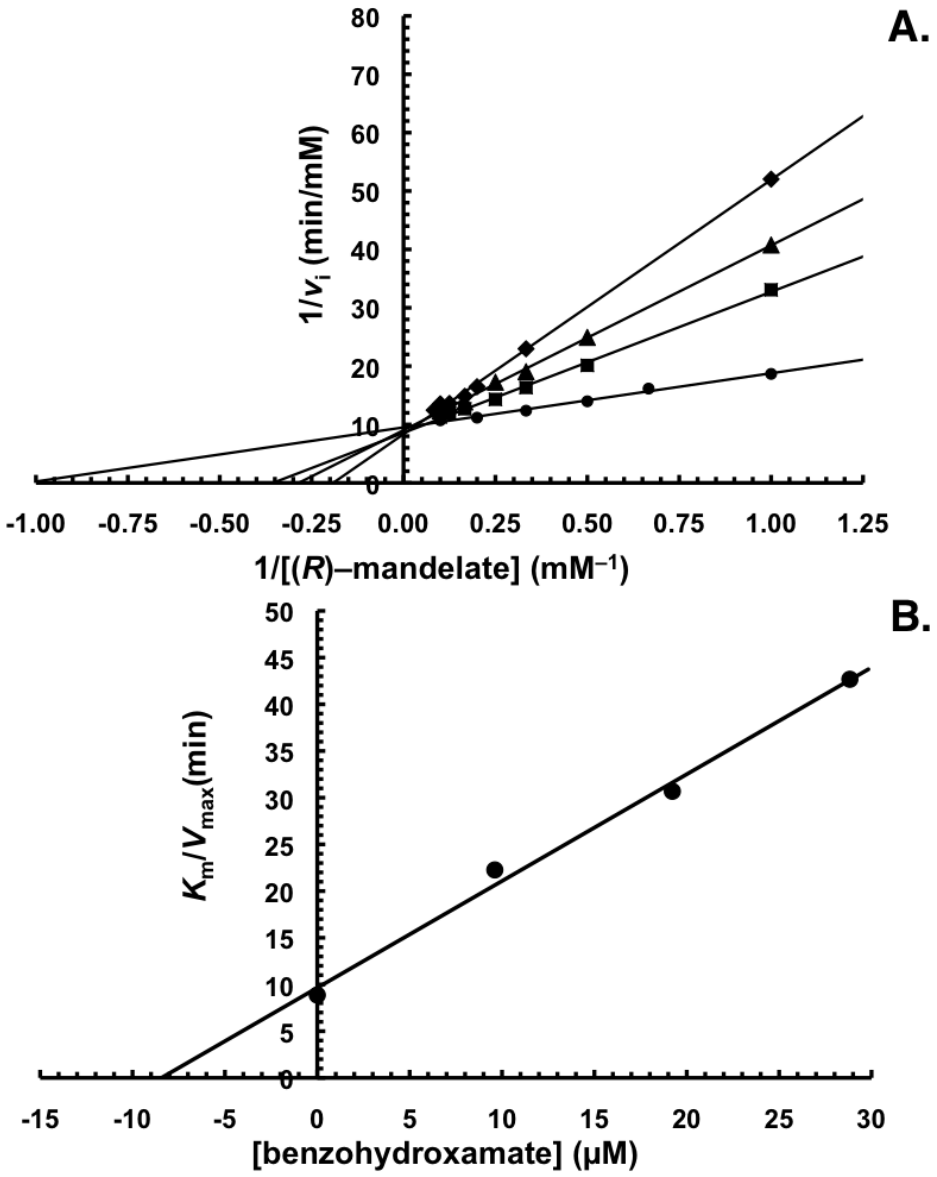

Supplementary Figure S8. A representative double reciprocal plot for the competitive inhibition of Co^{2+}-bound MR by BzH (**A**) and replot of $(K_m/V_{max})^{app}$ as a function of free BzH concentrations (**B**). (**A**) Initial concentrations of (*R*)-mandelate ranged between values of 1.00 mM and 10.00 mM. Concentrations of total BzH used were 0 μM (●), 15 μM (■), 30 μM (▲), and 45 μM (◆). Assay conditions were as described in the Materials & Methods. (**B**) Plot of $(K_m/V_{max})^{app}$ values (determined from nonlinear regression analysis) as a function of free BzH concentrations ($[I]_{free}$ = 9.6, 19.2, and 28.8 μM) as determined by the method described in the Materials & Methods. The K_i value determined from these plots is 7.1 ± 0.3 μM.

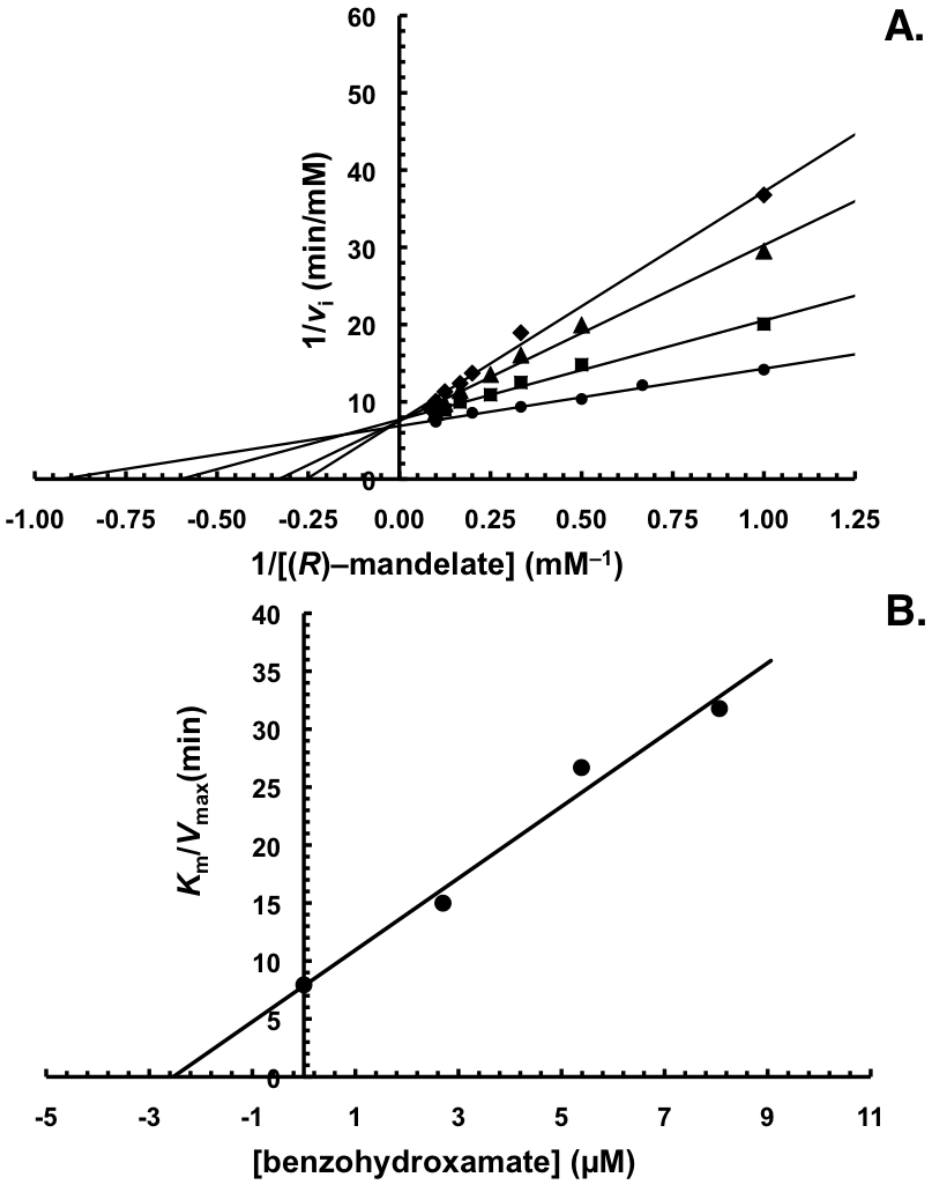

Supplementary Figure S9. A representative double reciprocal plot for the competitive inhibition of Ni^{2+}-bound MR by BzH (**A**) and replot of $(K_m/V_{max})^{app}$ as a function of free BzH concentrations (**B**). (**A**) Initial concentrations of (*R*)-mandelate ranged between values of 1.00 mM and 12.00 mM. Concentrations of total BzH used were 0 μM (●), 40 μM (■), 80 μM (▲), and 120 μM (◆). Assay conditions were as described in the Materials & Methods. (**B**) Plot of $(K_m/V_{max})^{app}$ (determined from nonlinear regression analysis) as a function of free BzH concentrations ($[I]_{free}$ = 2.7, 5.4, and 8.1 μM) as determined by the method described in the Materials & Methods. The K_i value determined from these plots is 2.7 ± 0.1 μM.

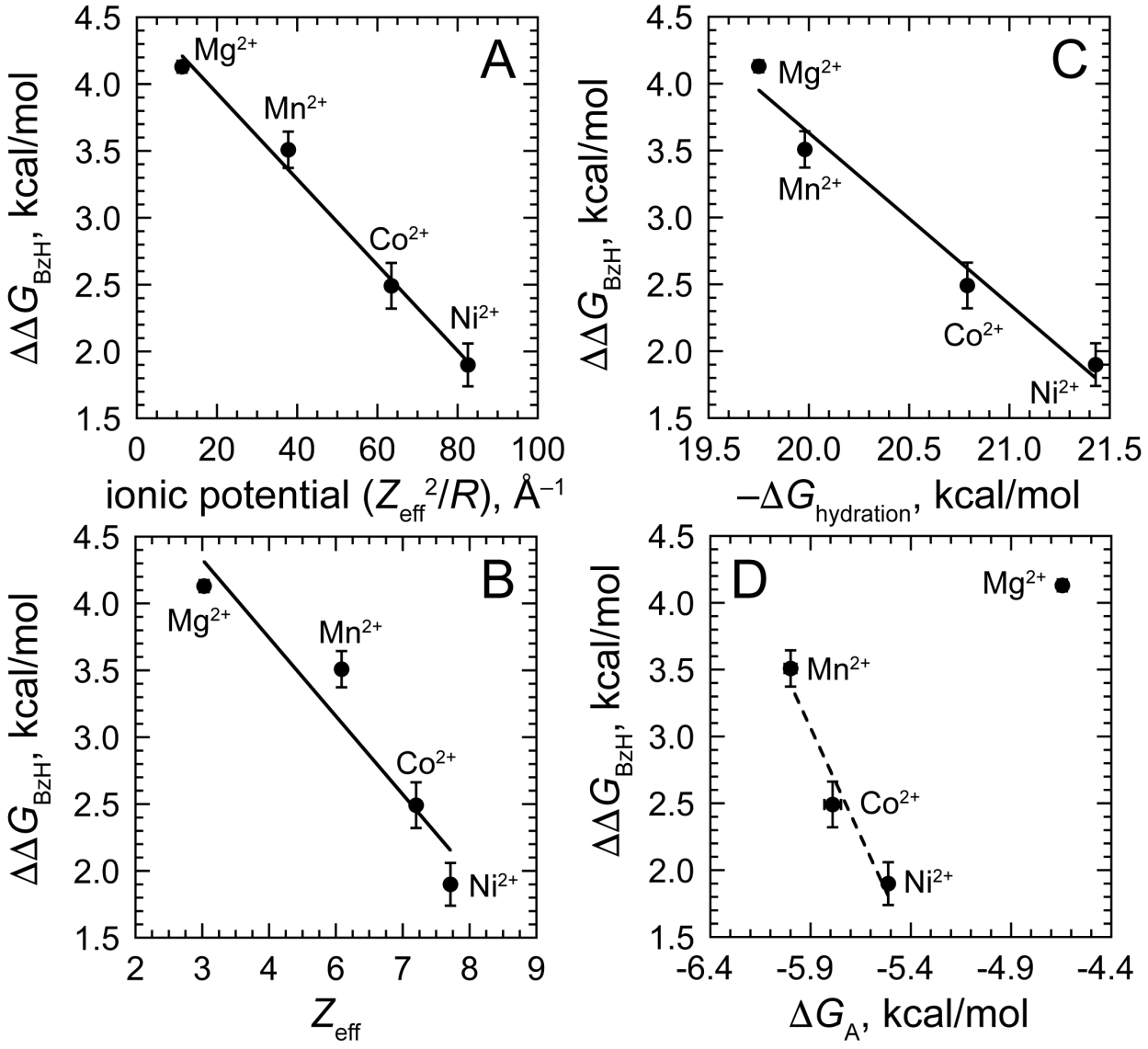

Supplementary Figure S10. Correlation of the free energy changes ($\Delta\Delta G_{BzH} = \Delta G_d - \Delta G_i$) of metal ion bound-MR (ΔG_i) and solution metal ion (ΔG_d) for BzH binding with the ionic potential (**A**, Z_{eff}^2/R, $R^2 = 0.9898$), effective nuclear charge (**B**, Z_{eff}, $R^2 = 0.8928$), the free energy for dehydration (**C**, $-\Delta G_{hydration}$, $R^2 = 0.9733$), and the free energy for metal ion binding to apo-MR (**D**, ΔG_A). *Cf*. **Fig. 6**. The Z_{eff} values were calculated using Slater's rules.[13]

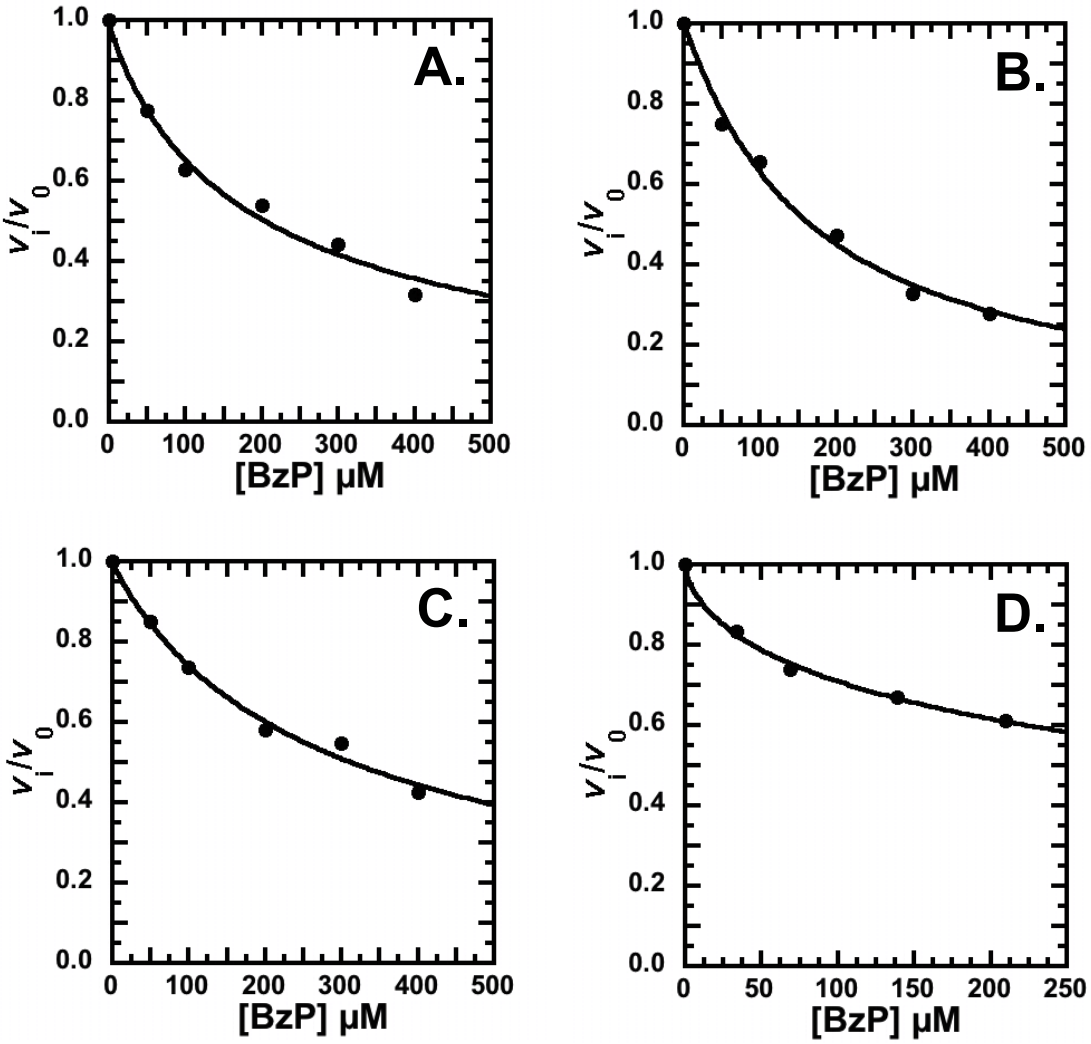

Supplementary Figure S11. Representative IC_{50} plots for the inhibition of Mg^{2+}- (**A**), Mn^{2+}- (**B**), Co^{2+}- (**C**), and Ni^{2+}-bound (**D**) MR by BzP. Initial concentrations of (*R*)-mandelate were 1.00 mM, 1.24 mM, 1.10 mM, and 1.00 mM for Mg^{2+}- (**A**), Mn^{2+}- (**B**), Co^{2+}- (**C**), and Ni^{2+}-bound (**D**) MR, respectively. Concentrations of BzP used were 50 – 400 μM for Mg^{2+}-, Mn^{2+}- and Co^{2+}-bound MR. The concentrations of free BzP ($[I]_{free}$) used for the estimation of the IC_{50} value for Ni^{2+}-bound MR were 34, 69, 139, and 210 μM, which were determined by the method described in the Materials & Methods. From the plots, the IC_{50} values were determined to be 202 ± 7, 193 ± 13, 308 ± 24, and 428 ± 16 μM (estimated by extrapolation) for Mg^{2+}-, Mn^{2+}-, Co^{2+}-, and Ni^{2+}-bound MR, respectively.

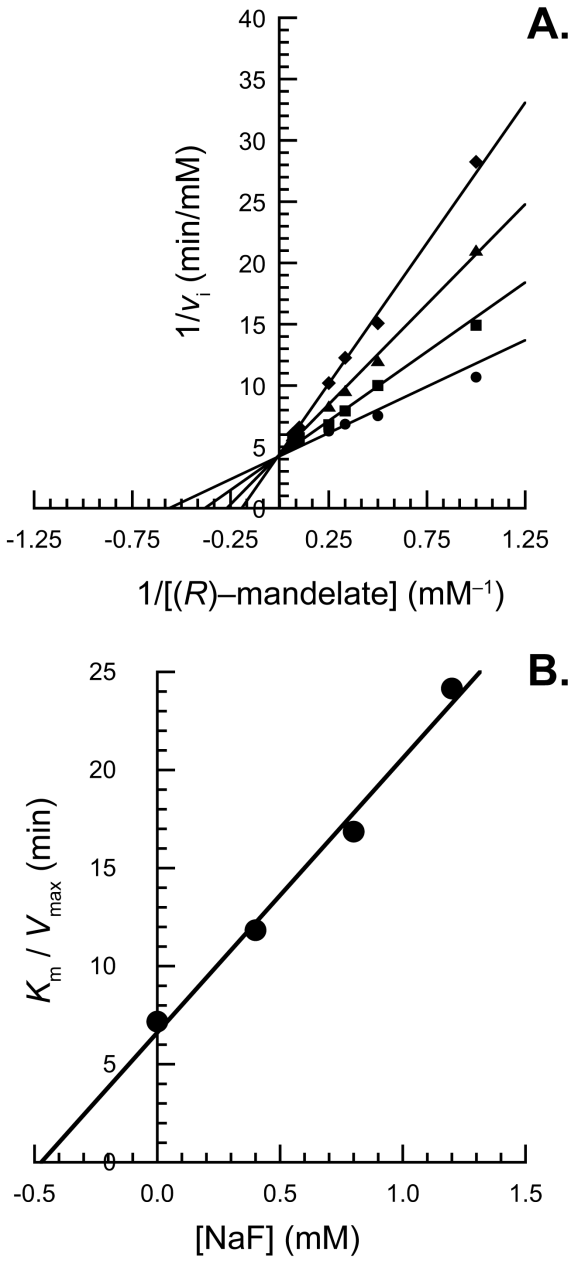

Supplementary Figure S12. A representative double reciprocal plot for the competitive inhibition of Mg^{2+}-bound MR by NaF (**A**) and replot of $(K_m/V_{max})^{app}$ as a function of NaF concentrations (**B**). (**A**) Initial concentrations of (*R*)-mandelate ranged between values of 0.5 mM and 15.0 mM. Concentrations of NaF used were 0 mM (●), 0.4 mM (■), 0.8 mM (▲), and 1.2 mM (◆). Assay conditions were as described in the Materials & Methods. (**B**) Plot of $(K_m/V_{max})^{app}$ (determined from nonlinear regression analysis) as a function of NaF yields an x-intercept equal to $-K_i$. The K_i value determined from these plots is 0.47 ± 0.03 mM.

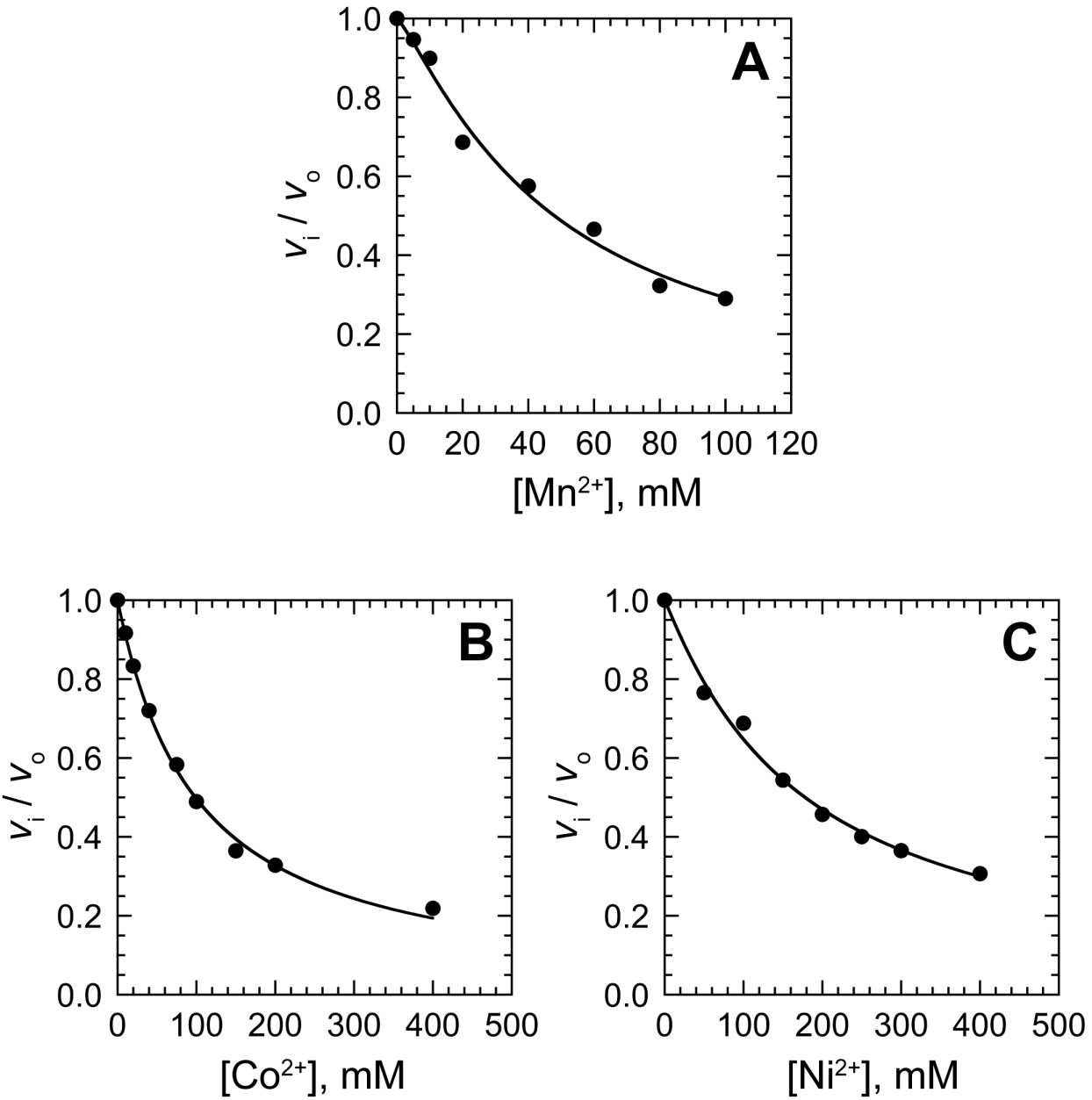

Supplementary Figure S13. Representative IC_{50} plots for the inhibition of Mn^{2+}- (**A**), Co^{2+}- (**B**), and Ni^{2+}-bound (**C**) MR by NaF. The concentration of (*R*)-mandelate was 1.00 mM. Concentrations of NaF used were 5 – 100 mM for Mn^{2+}-bound MR, 10 – 400 mM for Co^{2+}-bound MR, and 50 – 400 mM for Ni^{2+}-bound MR. From the plots, the IC_{50} values were determined to be 48 ± 4, 93 ± 5, and 178 ± 7 mM for Mn^{2+}-, Co^{2+}-, and Ni^{2+}-bound MR, respectively.

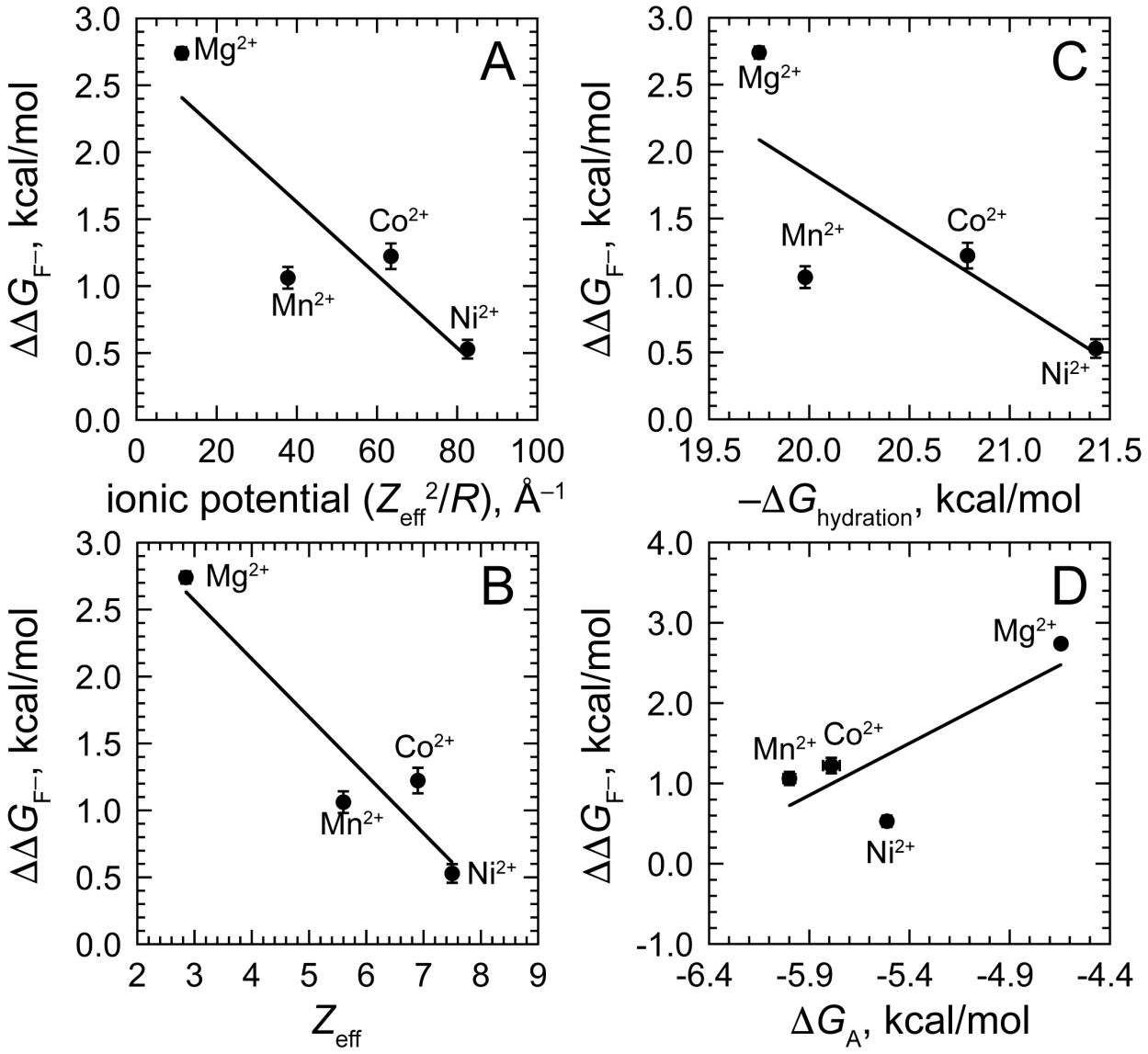

Supplementary Figure S14. Weak correlation of the free energy changes ($\Delta\Delta G_{F^-} = \Delta G_d - \Delta G_i$) of metal ion bound-MR (ΔG_i) and solution metal ion (ΔG_d) for fluoride ion binding with the ionic potential (**A**, Z_{eff}^2/R, $R^2 = 0.8205$), effective nuclear charge (**B**, Z_{eff}, $R^2 = 0.9121$), the free energy for dehydration (**C**, $-\Delta G_{hydration}$, $R^2 = 0.6296$), and the free energy for metal ion binding to apo-MR (**D**, ΔG_A, $R^2 = 0.6609$). *Cf*. **Fig. 6**. The Z_{eff} values were calculated using Slater's rules.[13]

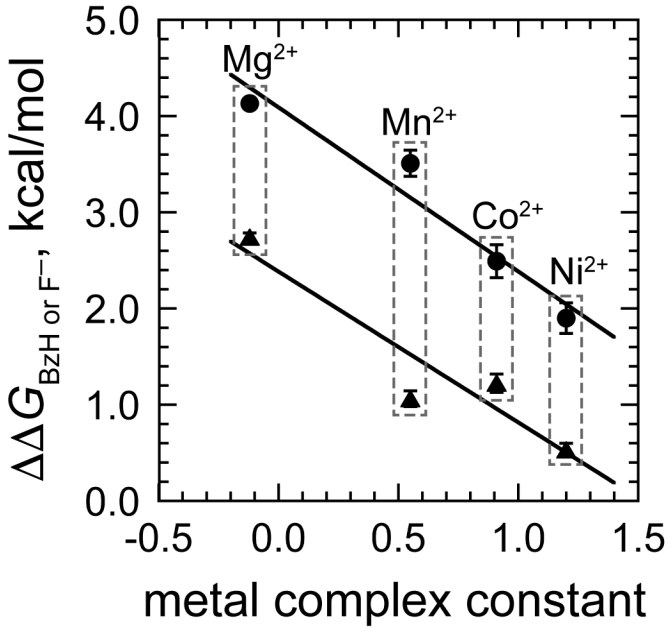

Supplementary Figure S15. Differences in free energy for the binding of BzH and fluoride anion at the active site of the metal ion variants of MR and in aqueous solution ($\Delta\Delta G_{ligand}$) as a function of the metal complex constants (MC). The values of $\Delta\Delta G_{BzH}$ (●, $R^2 = 0.9411$) and $\Delta\Delta G_{F^-}$ (▲, $R^2 = 0.8848$) are plotted as a function of the MC values developed by Martin[24] for comparing the relative ability of metals to form complexes. See **ESI,† Table S2** for values.

REFERENCES

1 J. K. Grady, N. D. Chasteen and D. C. Harris, Radicals from "Good's" buffers, *Anal. Biochem.*, 1988, **173**, 111-115.

2 B. Tadolini, Iron autoxidation in Mops and Hepes buffers, *Free Radic. Res. Commun.*, 1987, **4**, 149-160.

3 K. D. Welch, T. Z. Davis and S. D. Aust, Iron autoxidation and free radical generation: effects of buffers, ligands, and chelators, *Arch. Biochem. Biophys.*, 2002, **397**, 360-369.

4 R. D. Shannon, Revised effective ionic radii and systematic studies of interatomic distances in halides and chalcogenides, *Acta Cryst.*, 1976, **A32**, 751-767.

5 I. Marcus, Ionic radii in aqueous solutions, *Chem. Rev.*, 1988, **88**, 1475-1498.

6 I. Persson, Hydrated metal ions in aqueous solution: How regular are their structures, *Pure Appl. Chem.*, 2010, **82**, 1901-1917.

7 M. Bucher and T. L. Porter, Analysis of the Born model for hydration of ions, *J. Phys. Chem.*, 1986, **90**, 3406-3411.

8 A. M. Romani, Cellular magnesium homeostasis, *Arch. Biochem. Biophys.*, 2011, **512**, 1-23.

9 V. L. Schramm and F. C. E. Wedler, *Manganese in metabolism and enzyme function*, Academic Press, Orlando, Fl., 1986.

10 M. Odaka and M. Kobayashi, in Encyclopedia of metalloproteins, eds. R. H. Kretsinger, V. N. Uversky and E. A. Permyakov, Springer, New York, 2013, p. 670.

11 Y. Li and D. B. Zamble, Nickel homeostasis and nickel regulation: an overview, *Chem. Rev.*, 2009, **109**, 4617-4643.

12 R. G. Pearson, Absolute electronegativity and hardness: Application to inorganic chemistry, *Inorg. Chem.*, 1988, **27**, 734-740.

13 J. C. Slater, Atomic shielding constants, *Phys. Rev.*, 1930, **36**, 57-64.

14 V. R. Williams and J. Selbin, Divalent metal ion activation of β-methylaspartase, *J. Biol. Chem.*, 1964, **239**, 1635-1639.

15 M. Harty and S. L. Bearne, Measuring benzohydroxamate complexation with Mg^{2+}, Mn^{2+}, Co^{2+}, and Ni^{2+} using isothermal titration calorimetry, *J. Therm. Anal. Calorim.*, 2015, **123**, 2573-2582.

16 S. P. Tanner, J. B. Walker and G. R. Choppin, Thermodynamic parameters of the alkaline earth monofluorides, *J. Inorg. Nucl. Chem.*, 1968, **30**, 2067-2070.

17 B. Elgquist and M. Wedborg, Stability constants of $NaSO_4^-$, $MgSO_4$, MgF^+, $MgCl^+$ ion pairs at the ionic strength of seawater by potentiometry, *Marine Chem.*, 1978, **6**, 243-252.

18 B. Elgquist, Determination of the stability constants of MgF^+ and CaF^+ using a fluoride ion selective electrode, *J. Inorg. Nucl. Chem.*, 1970, **32**, 937-944.

19 L. Ciavatta and M. Grimaldi, On the complex formation between manganese (II) and fluoride ions, *J. Inorg. Nucl. Chem.*, 1965, **27**, 2019-2025.

20 A. M. Bond and G. Hefter, A study of the weak fluoride complexes of the divalent first row transition metal ions with fluoride ion-selective electrode, *J. Inorg. Nucl. Chem.*, 1972, **34**, 603-607.

21 S. Ahrland and K. Rosengren, The stability of metal halide complexes in aqueous solution II. The fluoride complexes of divalent nickel, copper, and zinc, *Acta Chem. Scand.*, 1956, **10**, 727-734.

22 A. E. Martell, R. M. Smith and R. J. Motekaitis, *NIST Critically selected stability constants of metal complexes*, Gaithersburg, MD, 2001.

23 G. Anderegg, Critical survey of stability constants of NTA complexes, *Pure Appl. Chem.*, 1982, **54**, 2693-2758.

24 B. L. Martin, Development of a scale for the comparison of metals in enzyme action, *J. Inorg. Biochem.*, 1999, **75**, 245-254.

25 K. Schneider, H. G. Schlegel and K. Jochim, Effect of nickel on activity and subunit composition of purified hydrogenase from *Nocardia opaca* 1b, *Eur. J. Biochem.*, 1984, **138**, 533-541.

26 S. G. Powers and E. E. Snell, Ketopantoate hydroxymethyltransferase II. Physical, catalytic, and regulatory properties, *J. Biol. Chem.*, 1976, **251**, 3786-3793.

27 S. Kurz, J. G. King, R. R. Dinglasan, K. Paschinger and I. B. Wilson, The fucomic potential of mosquitoes: Fucosylated *N*-glycan epitopes and their cognate fucosyltransferases, *Insect Biochem. Mol. Biol.*, 2016, **68**, 52-63.

28 J. H. Veerkamp, Biochemical changes in *Bifidobacterium bifidum var. pennsylvanicus* after cell-wall inhibition. VI. Biosynthesis of the galactosyldiglycerides, *Biochim. Biophys. Acta*, 1974, **348**, 23-34.

29 S. Cunha, A. F. d'Avó, A. Mingote, P. Lamosa, M. S. da Costa and J. Costa, Mannosylglucosylglycerate biosynthesis in the deep-branching phylum *Planctomycetes*: characterization of the uncommon enzymes from *Rhodopirellula baltica*, *Sci. Rep.*, 2013, **3**, 2378.

30 W. K. Chou, S. Dick, W. W. Wakarchuk and M. E. Tanner, Identification and characterization of NeuB3 from C*ampylobacter jejuni* as a pseudaminic acid synthase, *J. Biol. Chem.*, 2005, **280**, 35922-35928.

31 M. R. Grace, C. T. Walsh and P. A. Cole, Divalent ion effects and insights into the catalytic mechanism of protein tyrosine kinase Csk, *Biochemistry*, 1997, **36**, 1874-1881.

32 J. Reimann, D. Esser, A. Orell, F. Amman, T. K. Pham, J. Noirel, A. C. Lindås, R. Bernander, P. C. Wright, B. Siebers and S. V. Albers, Archaeal signal transduction: impact of protein phosphatase deletions on cell size, motility, and energy metabolism in *Sulfolobus acidocaldarius*, *Mol. Cell. Proteomics*, 2013, **12**, 3908-3923.

33 M. L. Fonda and Y. Zhang, Kinetic mechanism and divalent metal activation of human erythrocyte pyridoxal phosphatase, *Arch. Biochem. Biophys.*, 1995, **320**, 345-352.

34 R. Xing and W. B. Whitman, Characterization of enzymes of the branched-chain amino acid biosynthetic pathway in *Methanococcus* spp., *J. Bacteriol.*, 1991, **173**, 2086-2092.

35 W. S. Yew, A. A. Fedorov, E. V. Fedorov, S. C. Almo and J. A. Gerlt, Evolution of enzymatic activities in the enolase superfamily: L-talarate/galactarate dehydratase from *Salmonella typhimurium* LT2, *Biochemistry*, 2007, **46**, 9564-9577.

36 J. Carere, S. E. McKenna, M. S. Kimber and S. Y. Seah, Characterization of an aldolase-dehydrogenase complex from the cholesterol degradation pathway of *Mycobacterium tuberculosis*, *Biochemistry*, 2013, **52**, 3502-3511.

37 M. Kataoka, M. Ikemi, T. Morikawa, T. Miyoshi, K. Nishi, M. Wada, H. Yamada and S. Shimizu, Isolation and characterization of D-threonine aldolase, a pyridoxal-5′-phosphate-dependent enzyme from *Arthrobacter* sp. DK-38, *Eur. J. Biochem.*, 1997, **248**, 385-393.

38 S. Friedmann, B. E. Alber and G. Fuchs, Properties of *R*-citramalyl-coenzyme A lyase and its role in the autotrophic 3-hydroxypropionate cycle of *Chloroflexus aurantiacus*, *J. Bacteriol.*, 2007, **189**, 2906-2914.

39 J. Wang, Y. Okamoto, K. Tsuboi and N. Ueda, The stimulatory effect of phosphatidylethanolamine on N-acylphosphatidylethanolamine-hydrolyzing phospholipase D (NAPE-PLD), *Neuropharmacology*, 2008, **54**, 8-15.

40 L.-P. B. Han, C. M. Schimandle, L. M. Davison and D. L. Vander Jagt, Comparative kinetics of Mg^{2+}, Mn^{2+}, Co^{2+}, and Ni^{2+}-activated glyoxalase I. Evaluation of the role of the metal ion, *Biochemistry*, 1977, **16**, 5478-5484.

41 S. Lee and C. D. Poulter, *Escherichia coli* type I isopentenyl diphosphate isomerase: structural and catalytic roles for divalent metals, *J. Am. Chem. Soc.*, 2006, **128**, 11545-11550.

42 E. Kourtoglou, G. E. Anasontzis, D. Mamma, E. Topakas, D. G. Hatzinikolaou and P. Christakopoulos, Constitutive expression, purification and characterization of a phosphoglucomutase from *Fusarium oxysporum*, *Enzyme Microb. Technol.*, 2011, **48**, 217-224.

43 K. Nakamura, Y. Shirokane and M. Suzuki, Purification and some properties of β-phosphoglucomutase from *Lactobacillus lactis* subsp. *cremonis* IFP 3427, *J. Ferment. Bioeng.*, 1998, **85**, 350-353.

44 A. Kim, J. Kim, B. M. Martin and D. Dunaway-Mariano, Isolation and characterization of the carbon-phosphorus bond-forming enzyme phosphoenolpyruvate mutase from the mollusk *Mytilus edulis*, *J. Biol. Chem.*, 1998, **273**, 4443-4448.

45 W. Mu, F. Chu, Q. Xing, S. Yu, L. Zhou and B. Jiang, Cloning, expression, and characterization of a D-psicose 3-epimerase from *Clostridium cellulolyticum* H10, *J. Agric. Food Chem.*, 2011, **59**, 7785-7792.

46 W. Mu, W. Zhang, D. Fang, L. Zhou, B. Jiang and T. Zhang, Characterization of a D-psicose-producing enzyme, D-psicose 3-epimerase, from *Clostridium* sp., *Biotechnol. Lett.*, 2013, **35**, 1481-1486.

47 C. Ingram-Smith and K. S. Smith, AMP-forming acetyl-CoA synthetases in Archaea show unexpected diversity in substrate utilization, *Archaea*, 2006, **2**, 95-107.

48 B. C. Shenoy and H. G. Wood, Purification and properties of the synthetase catalyzing the biotination of the aposubunit of transcarboxylase from *Propionibacterium shermanii*, *FASEB J.*, 1988, **2**, 2396-2401.